Deep-sea water displacement from a turbidity current induced by the Super Typhoon Hagibis

Shinsuke Kawagucci [Corresp., 1, 2], **Tetsuya Miwa** [2, 3], **Dhugal J Lindsay** [4, 5], **Eri Ogura** [4, 5], **Hiroyuki Yamamoto** [2, 6], **Kenichiro Nishibayashi** [7], **Hiroyuki Yokooka** [7], **Shotaro Nishi** [7], **Ayu Takahashi** [8], **Sangkyun Lee** [8]

[1] Super-cutting-edge Grand and Advanced Research (SUGAR) Program, Institute for Extra-cutting-edge Science and Technology Avant-garde Research (X-star), Japan Agency for Marine-Earth Science and Technology (JAMSTEC), Yokosuka, Japan

[2] Project team for developing innovative technologies for exploration of deep-sea resources, Japan Agency for Marine-Earth Science and Technology (JAMSTEC), Tokyo, Japan

[3] Institute for Marine-Earth Exploration and Engineering (MarE3), Japan Agency for Marine-Earth Science and Technology (JAMSTEC), Yokosuka, Japan

[4] Institute for Extra-cutting-edge Science and Technology Avant-garde Research (X-star), Advanced Science-Technology Research (ASTER) Program, Japan Agency for Marine-Earth Science and Technology (JAMSTEC), Yokosuka, Japan

[5] Graduate School of Nanobioscience, Yokohama City University, Yokohama, Japan

[6] Research Institute for Global Change (RIGC), Marine Biodiversity and Environmental Assessment Research Center (BioEnv), Japan Agency for Marine-Earth Science and Technology (JAMSTEC), Yokosuka, Japan

[7] Research and Development Partnership for Next Generation Technology of Marine Resources Survey (J-MARES)/ IDEA Consultants, Tokyo, Japan

[8] Research and Development Partnership for Next Generation Technology of Marine Resources Survey (J-MARES) / JGI, Inc., Tokyo, Japan

Corresponding Author: Shinsuke Kawagucci
Email address: kawagucci@jamstec.go.jp

Turbidity currents are themain drivers behind the transportation of terrestrial sediments to the deep sea, and turbidite deposits from such currents have been widely used in geological studies. Nevertheless, the contribution of turbidity currents to vertical displacement of seawater has rarely beendiscussed. This is partly because until recently, deep-sea turbidity currents have rarely been observed due to their unpredictable nature, being usually triggered by meteorological or geological events such as typhoons and earthquakes. Here, we report a direct observation of a deep-sea turbidity current using the recently developed Edokko Mark 1 monitoring system deployed in 2019 at a depth of 1,370 m in Suruga Bay, central Japan. A turbidity current occurred two days after its probable cause, the Super Typhoon Hagibis (2019), passed through Suruga Bay causing devastating damage. Over aperiod of 40 hours, we observed increased turbidity with turbulentconditions confirmed by a video camera. The turbidity exhibited two sharp peaks around 3:00 and 11:00 onOctober 14 (Japan Standard Time). The temperature and salinity characteristics during these high turbidity events agreed with independent measurements for shallow water layers in Suruga Bay at the same time, strongly suggesting that the turbidity current caused vertical displacement in the bay's water column by transporting warmer and shallower waters downslope of the canyon. Our results add to the previous few examples thatshow meteorological and geological events may have significant

contributions in the transportation of shallower seawater to the deep sea. Recent technological developments pertaining to theEdokko Mark 1 and similar devices enable straightforward, long-term monitoring of the deep-seafloor and will contribute to the understanding of similar spontaneous events in the deep ocean.

Deep-sea water displacement from a turbidity current induced by the Super Typhoon Hagibis

Shinsuke KAWAGUCCI[1,2], Tetsuya MIWA[2,3], Dhugal LINDSAY[4,5], Eri OGURA[4,5], Hiroyuki YAMAMOTO[2,6], Ken-ichiro NISHIBAYASHI[7], Hiroyuki YOKOOKA[7], Shotaro NISHI[7], Ayu TAKAHASHI[8], Sangkyun LEE[8]

[1] Japan Agency for Marine-Earth Science and Technology (JAMSTEC), Institute for Extra-cutting-edge Science and Technology Avant-garde Research (X-star), Super-cutting-edge Grand and Advanced Research (SUGAR) Program, 2-15 Natsushima-cho, Yokosuka, Japan
[2] Japan Agency for Marine-Earth Science and Technology (JAMSTEC), Project team for developing innovative technologies for exploration of deep-sea resources, 2-2-2 Uchisaiwaicho, Tokyo, Japan
[3] Japan Agency for Marine-Earth Science and Technology (JAMSTEC), Institute for Marine-Earth Exploration and Engineering (MarE3), MarE3, 2-15 Natsushima-cho, Yokosuka, Japan
[4] Japan Agency for Marine-Earth Science and Technology (JAMSTEC), Institute for Extra-cutting-edge Science and Technology Avant-garde Research (X-star), Advanced Science-Technology Research (ASTER) Program, 2-15 Natsushima-cho, Yokosuka, Japan
[5] Yokohama City University, Graduate School of Nanobioscience, 2-22 Seto, Yokohama Japan.
[6] Japan Agency for Marine-Earth Science and Technology (JAMSTEC), Research Institute for Global Change (RIGC), Marine Biodiversity and Environmental Assessment Research Center (BioEnv), 2-15 Natsushima-cho, Yokosuka, Japan
[7] Research and Development Partnership for Next Generation Technology of Marine Resources Survey (J-MARES)/ IDEA Consultants, Inc., 3-15-1 Komazawa, Setagaya-ku, Tokyo, Japan
[8] Research and Development Partnership for Next Generation Technology of Marine Resources Survey (J-MARES) / JGI, Inc., 1-5-21, Otsuka, Bunkyo-ku, Tokyo, Japan

Corresponding Author:
Shinsuke KAWAGUCCI[1]
2-15 Natsushima-cho, Yokosuka, 237-0061, JAPAN
Email address: kawagucci@jamstec.go.jp

Abstract

Turbidity currents are the main drivers behind the transportation of terrestrial sediments to the deep sea, and turbidite deposits from such currents have been widely used in geological studies. Nevertheless, the contribution of turbidity currents to vertical displacement of seawater has rarely been discussed. This is partly because until recently, deep-sea turbidity currents have rarely been observed due to their unpredictable nature, being usually triggered by meteorological or geological events such as typhoons and earthquakes. Here, we report a direct observation of a deep-sea turbidity current using the recently developed Edokko Mark 1 monitoring system deployed in 2019 at a depth of 1,370 m in Suruga Bay, central Japan. A turbidity current occurred two days after its probable cause, the Super Typhoon Hagibis (2019), passed through Suruga Bay causing devastating damage. Over a period of 40 hours, we observed increased turbidity with turbulent conditions confirmed by a video camera. The turbidity exhibited two sharp peaks around 3:00 and 11:00 on October 14 (Japan Standard Time). The temperature and salinity characteristics during these high turbidity events agreed with independent measurements for shallow water layers in Suruga Bay at the same time, strongly suggesting that the turbidity current caused vertical displacement in the bay's water column by transporting warmer and shallower waters downslope of the canyon. Our results add to the previous few examples that show meteorological and geological events may have significant contributions in the transportation of shallower seawater to the deep sea. Recent technological developments pertaining to the Edokko Mark 1 and similar devices enable straightforward, long-term monitoring of the deep-seafloor and will contribute to the understanding of similar spontaneous events in the deep ocean.

Introduction

Turbidity currents are particle-laden, gravity-driven flows that efficiently transport terrigenous sediment and organic matter, as well as benthic fauna and microplastics, to the deep sea [Meiburg & Kneller 2010; Sen et al. 2017; Pohl et al. 2020]. The damaging of seafloor fiber-optic cables by turbidity currents causes serious disruption of social activities [Pope et al. 2017]. The sedimentary deposits resulting from turbidity currents are known as turbidites and have been widely used in geological studies [e.g. Piper & Normark 2009]. For example, dating of the repeated turbidite sequences in the accretionary prism provide decisive evidence for tectonic evolution at the convergent plate boundary [Taira 2001]. Despite these multidimensional interests, direct observation of turbidity currents in the deep sea had been rare until the beginning of this century [Talling et al. 2013] due to their unpredictable nature and the limited accessibility resulting from challenges and ship time costs of deep-sea expeditions although numbers of the observation have increased during the last decade [Xu, 2010; Liu et al., 2012; Khripounoff et al., 2012; Hughes Clarke, 2019; Paull et al., 2018; Wang et al., 2020; Heerema et al., 2020; Hage et al., 2019; Normandeau et al., 2020; Lintern et al., 2016; Simmons et al., 2020].

Limited *in situ* direct observations provide the only clues to understand the possible impacts of deep-sea turbidity currents. To date, oceanographic CTD sensors deployed on seafloor observatories have revealed seawater temperature increases associated with deep-sea turbidity currents [Khripounoff et al. 2012; Wang et al. 2020]. A deep-sea mooring observatory off Taiwan has repeatedly captured typhoon-triggered turbidity currents and subsequent temperature increases over a period of 3.5 years [Zhang et al. 2018]. Cabled observatories placed on the deep seafloor have also captured turbidity currents triggered by earthquakes, such as at the Kuril subduction zone [Mikada et al. 2006] and off Hatsushima Island in central Japan [Kasaya et al. 2009]. These observations were coupled with temperature increases, suggesting low-density, shallow seawater were transported into deep depths as the interstitial water of turbidity currents, against the density stratification of the water column [Kao et al. 2010]. However, whether or not turbidity currents routinely cause such vertical displacement of seawater remains unclear due to the limited number of observations.

In addition to earthquakes, powerful tropical cyclones can also provide opportunities for the direct observation of deep-sea turbidity currents [e.g. Liu et al. 2012; Pope et al. 2017; Sequeiros et al. 2019]. On October 12 in 2019 (all timestamps in this paper are presented in JST: Japan Standard Time, UTC+9:00), the extremely large Super Typhoon Hagibis (2019) struck the main island of Japan, leading to a total of 86 deaths [Fire and Disaster Management Agency 2019] and the cancellation of three Rugby World Cup matches. Hagibis reached its peak intensity with a minimum atmospheric pressure of 915 hPa over the Philippine Sea on October 7, and passed through Suruga Bay with an atmospheric pressure of 955 hPa at 18:00 on October 12 (Figure 1A) [Japan Meteorological Agency 2019a]. During the passing of Hagibis, a maximum sea-level

96 departure of 224 cm and a 24-hour cumulative precipitation of up to 760 mm per m^2 were
97 recorded on the Izu Peninsula on the east coast of Suruga Bay, and a warning for severe flooding
98 was issued for the riverine area until the morning of October 13 [Shizuoka Local Meteorological
99 Office 2019; Takemi and Unuma 2020]. A global seafloor cable-break database analysis
100 demonstrated that tropical cyclones can trigger deep-sea turbidity currents several days after the
101 cyclone's passing [Pope et al. 2017]. We thus attempted a direct observation of the Hagibis-
102 linked deep turbidity current in Suruga Bay two days after the passing of Hagibis. Here, we
103 report visual and oceanographic properties of this *in situ* turbidity current, captured by the free-
104 fall-type deep-sea observatory system Edokko Mark 1 (Figure 2).
105
106

107 **Materials & Methods**
108
109 The Edokko Mark 1 (Type HSG) is an all-in-one, free-fall, stand-alone deep-sea monitoring
110 system [Miwa et al. 2015, Japan Agency for Marine-Earth Science and Technology 2017],
111 provided by Okamoto Glass Co. Ltd. (https://ogc-jp.com/en/). The Edokko Mark 1 and other
112 similar systems [Gallo et al. 2020; Clare et al. 2020] increase our capability for the observation
113 of deep-sea turbidity currents when typhoons, earthquakes, or tsunamis impact marginal seas.
114
115 The Edokko Mark 1 has a main frame with three glass spheres containing the main computer,
116 HD video cameras, 2400-4000 lumen LED lights, transponder, and batteries. The main frame is
117 further equipped with an acoustic releaser for the ballast weight at the base, a floating glass
118 sphere with a radio beacon and flasher at the top, and a 75 cm long, 50 cm wide PVC arm for
119 image-based measurements in the front (Figure 2). Edokko Mark 1 is capable of monitoring for
120 up to three months, owing to reduced battery consumption from a programmable long-term
121 monitoring mode allowing intermittent, periodic observations. In this study, Edokko Mark 1's
122 electric system was continuously powered until 15:23 on 14 October, after which it entered a
123 long-term monitoring mode with observations carried out for 1 minute every 30 minutes until
124 shipboard recovery at 10:20 on 16 October. In the set up used in the present study, a CTD
125 profiler (RINKO profiler, JFE Advantech) and a turbidity meter (ASTD2XTU, JFE Advantech
126 Co., Ltd.) were further attached to the main frame at 1.2 m above the seafloor (Figure 2). The
127 unit of turbidity, FTU (formazine turbidity unit), is defined as 1 FTU = turbidity where 1 mg of
128 formazin is homogeneously suspended in 1 L of water.
129
130 Edokko Mark 1 landed on the seafloor at a depth of 1,370 m at the mouth of Heda Canyon, in the
131 northeastern region of Suruga Bay (35°59.63'N - 138°40.30'E). The topography of Heda Canyon
132 is characterized by a narrow and winding valley (Figure 1B) that suggests the repeated
133 occurrence of deep-sea turbidity currents in the past [e.g. Azpiroz-Zabala et al. 2017], probably
134 associated with floods from the Heda River located on the Izu Peninsula (Figure 1A).
135

136   Still images were extracted from the video recordings at a 1 Hz frequency using OpenCV (cv2)
137   within a custom-built Python script (https://github.com/dhugallindsay/Image-based-turbidity-
138   flow-detection). Each 1 minute-long recording event contained several seconds at the beginning
139   when the lighting conditions were unstable just after power supply started. Care was taken
140   during the image extraction to set the start and end times to include only the time period for
141   which lights were on and the illumination was stable. A total of 49 images were extracted from
142   each 1-min recording-interval movie (.mpeg) file. The brightness values (0-255) for each color
143   channel (red, green, blue: RGB) were calculated for each and every pixel in the image and the
144   average values for each channel were then combined using the following formula: L =
145   B*0.114478+G*0.586611+R*0.298912, where L is luminance, according to the International
146   Telecommunication Union standard ITU-R BT.601 [International telecommunication Union
147   2011]. An average luminance value was then calculated for each image by averaging the values
148   for all pixels, and the 49 values for the 49 images were then averaged to calculate the average
149   luminance of each 49 second-long video file.

151   A vertical profile of seawater properties at the deployment location for the Edokko Mark 1 was
152   made using a XCTD profiler (XCTD-4, Tsurumi-Seiki Co., Ltd.). For a comparison to the
153   baseline, a CTD data profile, RF-6374 (34°39.12'N - 137°00.71'E), was derived from open data
154   of the 50-years 137°E hydrographic section maintained by the Japan Meteorological Agency
155   [e.g. Oka et al. 2018; Japan Meteorological Agency 2019b].

Results

160   The 40 hours of intermittent monitoring with Edokko Mark 1 successfully detected *in situ* deep-
161   sea turbidity currents, probably associated with Typhoon Hagibis. Edokko Mark 1 monitored and
162   recorded the temporal variation of pressure, turbidity, temperature, and salinity (Figure 3), as
163   well as recording video images (Figures 4 and 5) (Supplementary Video File). Oscillation of
164   water pressure at the seafloor corresponded to the tidal cycle, while the approximate mean
165   pressure of 14.05 MPa represents the water depth of 1,370 m where the Edokko Mark 1 was
166   deployed.

168   Seawater turbidity varied drastically during the observation period (Figure 3). The turbidity
169   stayed at a low level between 1-5 FTU with slight fluctuations until the end of October 14. From
170   00:55 to 14:55 of October 15, a high turbidity of >10 FTU was observed. Eventual spikes over
171   50 FTU were recorded at 02:55-04:26 and 11:26-11:56, hereafter referred to as the AM3 event
172   and AM11 event, respectively. There was a relatively calmer period between 07:55-10:56. After
173   14:55 of 15 October, the turbidity again dropped to a low level until the observation ended on
174   October 16. The timings of turbidity increment at 00:55 and the AM3 event corresponded to

175   those of the low tide, while the turbidity peak of the AM3 event was 3 hours after the last low
176   tide.
177
178   Magnitude of seawater cloudiness in the video images recorded by the camera (Figures 4, 5)
179   corresponded well to turbidity levels recorded by the turbidity sensor (Figure 3). At 00:26 on 15
180   October, the horizontal bars of the Edokko Mark 1's arm, located 30 cm away from the front of
181   the main body, can be identified (Figure 4A). During the period from 00:56 on 15 October,
182   where strong turbidity was detected, video images confirmed a storm of brownish particles and
183   the bars became indiscernible (Figure 4B, 4C). When the turbidity reached over 100 FTU at
184   03:56, the video camera blacked out (Figure 4D, 4E), suggesting that the turbidity current struck
185   the camera and light on Edokko Mark 1 after 03:26. Following a relatively calm period (Figure
186   4F, 4G), another black-out situation occurred at 11:26 on 15 October during the AM11 event,
187   when the video camera captured the moment where a turbidity current struck the Edokko Mark 1
188   (Figures 4H, 5) (Supplementary Video File). After 13:55 on 15 October, when turbidity values
189   were lower than 10 FTU, the arm was again identifiable in the video images (Figure 4I, 4J, 4K).
190   The RGB characteristics of the images demonstrated a decrease in blue component when the
191   seawater turbidity increased (Figure 3), indicating the predominance of brownish particles.
192
193   Both temperature and salinity, monitored by the Edokko Mark 1, were not stable during the
194   observation period. The temporal variations of temperature and salinity generally yielded a
195   mirror image of each other, even during the temperature peak at 02:55-03:26 on 15th October, in
196   the AM3 event (Figure 3) just before the extreme turbidity over 100 FTU was recorded at 03:55.
197   At the AM11 event, however, only salinity decreased while temperature remained relatively
198   stable. The degree of variation seen in both temperature and salinity were large leading up to the
199   AM11 event, and became more stable after that. Quantitatively, the mean temperature (shown
200   with standard deviation) before the AM11 event was 2.78±0.04 ℃ and 2.83±0.02 ℃ after it. The
201   mean salinity, on the other hand, was 34.485±0.005 before the AM11 event and 34.478±0.002
202   after. Note that the temperature and salinity data during the AM3 and AM11 events were
203   eliminated from the calculation. The decreases in salinity, measured by conductivity using the
204   CTD, were observed during the high turbidity events. These are attributable not only to seawater
205   with lower salinity, but also to increased concentration of suspended particles due to suspended
206   particles being less conductive than seawater [e.g. Wang et al. 2020]. On the other hand, the
207   thermometer is inert to the changes in concentrations of suspended particles and was thus
208   unaffected.
209
210   The relationships between the timing of low tide, increase in turbidity and temperature, and
211   video capture of destructive turbidity current differed between AM3 and AM11 events. Before
212   the AM3 event, the lowest tide occurred at midnight and was followed by increase in turbidity at
213   around 01:00 and temperature at around 02:00 (Figure 3), both reaching highest values at the
214   AM3 event. Before the AM11 event which happened at the same time as a low tide, however, no

215 such signs were detected in the sensors prior to the visual confirmation of the turbidity current,
216 following which the turbidity declined consistently.
217
218 The characteristics of potential temperature and salinity observed by the Edokko Mark 1 during
219 the turbidity current observation generally agreed with those of the ambient water column at the
220 Edokko Mark 1's deployment locality, as observed by the XCTD, as well as the reliable
221 reference data RF-6374 (Figure 6). Slight offsets of potential temperature and salinity
222 characteristics among data from the Edokko Mark 1, XCTD, and RF-6374 are probably due to
223 the insufficient calibration of one or more devices. Consistencies in the trends of potential
224 temperature and salinity variation between the seafloor-deployed Edokko Mark 1 and vertical
225 profilers strongly suggests the displacement of the generally-stratified deep seawater around the
226 Edokko Mark 1. Outside the two events, the potential temperature and salinity values recorded
227 by the Edokko Mark 1 showed slight fluctuation and corresponded to those of the ambient deep-
228 seawater at 1,300-1,380 m depth observed by the XCTD, close to the seafloor depth of 1,370 m
229 (Figure 6). Potential temperature and salinity recorded by the Edokko Mark 1 during the AM3
230 event also followed the trend of the ambient seawater and corresponded to those of seawater
231 approximately 200 m shallower than Edokko Mark 1's location (Figure 6A-D). Although the
232 properties of the seawater during the AM3 event appears to be attributable to 1 % contribution of
233 surface seawater with a salinity of 31 and temperature of 25 °C into the bottom water (Figure
234 6E), the direct bimodal mixing between surface and bottom waters is unlikely due to some
235 mixing with seawater at intermediate depths during the downslope transportation being
236 inevitable. On the other hand, the potential temperature and salinity during the AM11 event are
237 too far deviated from those of the water column, suggesting false conductivity signals resulting
238 from the high concentration of suspended particles, as discussed above.
239
240
241 **Discussion**
242
243 Turbidity currents can be considered to be the driving force for the vertical stirring of deep-sea
244 water observed in the CTD data during this study, since, in general, low-density shallow
245 seawater cannot sink down to great depths without an external driving force. In support of this,
246 previous observations by cabled observatories have consistently recorded increases of seawater
247 temperature at the seafloor accompanied with turbidity currents [Mikada et al. 2006, Kasaya et
248 al. 2009, Zhang et al. 2018]. Since a turbidity current is a composite of sedimentary particles
249 suspended in a seawater matrix, the density is naturally higher than the density of interstitial
250 water alone and causes the shallow seawater to sink to great depths [Kao et al. 2010]. This
251 mechanism is the most plausible explanation for the current CTD observations by the Edokko
252 Mark 1. As interstitial water density of the typhoon-induced turbidity current during the AM3
253 event was approximately 0.05 kg/m^3 lower than that during periods outside of the two events
254 (Figure 6D), the turbidity current was able to obtain sufficient density from the suspended

255 particles. The suspended particles of >50 FTU, corresponding to 0.05 kg/m^3 under the model
256 definition (see Materials & Methods), can produce sufficient gravity in the whole turbidity
257 current, resulting in the sinking of seawater into the depths of Suruga Bay from at least 200 m
258 above the seafloor. We would, however, caution that the 1:1 model conversion of FTU to g/m^3 is
259 unlikely to be accurate for natural seawater due to variable densities of suspended particles.
260
261 The deep-sea turbidity current observed in this study was probably induced by the record-
262 breaking Super Typhoon Hagibis (2019). Although the deep-sea turbidity current observed here
263 occurred two days after Hagibis passed over Suruga Bay, it has previously been reported that
264 deep-sea turbidity current occurred even several days after a cyclone passes [Pope et al. 2017].
265 Although earthquake-induced deep-sea disturbances have been observed to date [Mikada et al.
266 2006; Kasaya et al., 2009; Kawagucci et al. 2012; Noguchi et al. 2012], no significant earthquake
267 (M>1) occurred around the Suruga Bay area during Edokko Mark 1's monitoring period. Even
268 though an M5 earthquake occurred at 200 km east of Suruga Bay at 18:00 on 12 October [JMA
269 2019], this is both too early and too far away to have been the cause for the turbidity current
270 observed in Suruga Bay by the Edokko Mark 1.
271
272 Pin-pointing the trigger mechanism for the deep-sea turbidity current observed herein is
273 challenging, due to the limited availability of information. The turbidity current was observed
274 from a single monitoring location and a single vertical point of the deployed system that could
275 not measure the direction and speed of the *in situ* current, with no supplemental observation at
276 the river and coast to confirm the exact time and location of the turbidity current release. A
277 known major trigger mechanism for the turbidity current associated with typhoon is river flood
278 [Liu et al. 2012; Lintern et al., 2016; Clare et al., 2016; Hage et al., 2019]. The torrential rainfall
279 from Hagibis on October 12 [Takemi and Unuma 2020] indeed resulted in intensive flooding of
280 rivers in the Izu Peninsula, subsequently flowing into the eastern part of Suruga Bay [Shizuoka
281 Local Meteorological Office 2019]. However, the water level of these rivers returned to normal
282 before the noon of October 13 [Shizuoka Local Meteorological Office 2019], over 24 hours
283 before the turbidity flow event we observed on October 15. This long lag suggests that the
284 flooding associated with Hagibis itself could not trigger the observed turbidity current. On the
285 other hand, turbidity in the river water may have remained high until October 15 after flooding
286 has ceased, and this hyperpycnal river flow could have continued to supply sufficient suspended
287 particles to trigger the turbidity current. If this combined with low tide at midnight of October 15
288 to trigger the turbidity current seen during the AM3 event, it would have had a horizontal
289 velocity of 1 m/s, estimated from the duration of 3 hours and the distance of approximately 11
290 km between the Heda river mouth and the location of our Edokko deployment (Figure 1A). This
291 is comparable with the typical velocity seen in turbidity currents [e.g. Khripounoff et al. 2012].
292 The seawater property demonstrating entrainment with seawater from 200 m shallower is also
293 not inconsistent with this trigger mechanism when located at a coastal region. Nevertheless, no
294 concrete evidence is available to verify this scenario.

295

296 Another possible trigger for the turbidity current observed is submarine slope failure. It has
297 previously been reported that the rapid accumulation of seafloor sediment associated with
298 tropical cyclones can eventually cause submarine slope failure, resulting in the runoff of a deep-
299 sea turbidity current, even several days after a cyclone passes [Pope et al. 2017]. The torrent of
300 flooding, muddy streams in the forest-rich Izu Peninsula up until the noon of October 13
301 delivered an unusually large amount of terrestrial soil into the seafloor of Suruga Bay, and a part
302 of this accumulation may be further transported into the deep sea before the start of our
303 observation on October 14. Such unconsolidated sediments could serve as precursors of the
304 turbidity current observed on October 15. Particularly, the turbidity current at the AM11 event
305 which occurred synchronously at low tide without changes in seawater properties would have
306 occurred locally, possibly triggered by a local slope failure around the Edokko Mark 1, rather
307 than being directly triggered by turbid waters from the river.

308

309

310 **Conclusions**
311 We successfully recorded a deep-sea turbidity current probably induced by the Super Typhoon
312 Hagibis and vertical stirring of deep-sea water due to this turbidity current, based on
313 observations by the easy-to-use, autonomous monitoring system Edokko Mark 1. These
314 spontaneous events are difficult to observe without *in situ* long-term monitoring, and this
315 capacity will help illuminate the diverse forms and mechanisms of turbidity currents in the deep
316 ocean.

317

318

319 **Acknowledgements**
320 Authors are grateful to Drs. Chong CHEN, Kazuya KITADA, Satoshi OSAFUNE, and Shiro
321 MATSUGAURA for supporting cruise operation, data processing, and manuscript editing. This
322 work was conducted as a part of Cross-ministerial Strategic Innovation Promotion Program (SIP)
323 "Innovative Technology for Exploration of Deep-Sea Resources" (Lead agency: JAMSTEC).
324 Authors deeply appreciate the cooperation of Pacific Islands' members who joined the capacity
325 building cruise of SIP.

326

327

328 **References**

329

330 Azpiroz-Zabala M., Cartigny M. J. B., Talling P. J., Parsons D. R., Sumner E. J., Clare M. A.,
331 Simmons S. M., Cooper C. and Pope E. L. (2017) Newly recognized turbidity current structure
332 can explain prolonged flushing of submarine canyons. *Science Advances* **3**, e1700200.

333

334 Clare M. A., Hughes Clarke J. E., Talling P. J., Cartigny M. J. B. and Pratomo D. G. (2016)
335 Preconditioning and triggering of offshore slope failures and turbidity currents revealed by most
336 detailed monitoring yet at a fjord-head delta. Earth and Planetary Science Letters 450, 208–220.
337

338 Clare M., Lintern D. G., Rosenberger K., Hughes Clarke J. E., Paull C., Gwiazda R., Cartigny
339 M. J. B., Talling P. J., Perara D., Xu J., Parsons D., Jacinto R. S. and Apprioual R. (2020)
340 Lessons learned from the monitoring of turbidity currents and guidance for future platform
341 designs. *Geological Society, London, Special Publications* **500**, 605–634.
342

343 Gallo, N. D., Hardy, K., Wegner, N. C., Nicoll, A., Yang, H., and Levin, L. A.: Characterizing
344 deep-water oxygen variability and seafloor community responses using a novel autonomous
345 lander, Biogeosciences Discuss., https://doi.org/10.5194/bg-2020-75, in review, 2020.
346

347 Hage S., Cartigny M. J. B., Sumner E. J., Clare M. A., Hughes Clarke J. E., Talling P. J., Lintern
348 D. G., Simmons S. M., Silva Jacinto R., Vellinga A. J., Allin J. R., Azpiroz-Zabala M., Gales J.
349 A., Hizzett J. L., Hunt J. E., Mozzato A., Parsons D. R., Pope E. L., Stacey C. D., Symons W. O.,
350 Vardy M. E. and Watts C. (2019) Direct Monitoring Reveals Initiation of Turbidity Currents
351 From Extremely Dilute River Plumes. Geophys. Res. Lett. 46, 11310–11320.
352

353 J., Talling P. J., Cartigny M. J., Paull C. K., Bailey L., Simmons S. M., Parsons D. R., Clare M.
354 A., Gwiazda R., Lundsten E., Anderson K., Maier K. L., Xu J. P., Sumner E. J., Rosenberger K.,
355 Gales J., McGann M., Carter L. and Pope E. (2020) What determines the downstream evolution
356 of turbidity currents? Earth and Planetary Science Letters 532, 116023–11.
357

358 Hughes Clarke J. E. H. (2019) First wide-angle view of channelized turbidity currents links
359 migrating cyclic steps to flow characteristics. Nature Communications, 1–13.
360

361 International Telecommunication Union (2011) Recommendation ITU-R BT.601-7 (Available
362 online at https://www.itu.int/dms_pubrec/itu-r/rec/bt/R-REC-BT.601-7-201103-I!!PDF-E.pdf.
363 accessed 30 June 2020).
364

365 Japan Agency for Marine-Earth Science and Technology (2017) JAMSTEC SIP Protocol Series
366 4: Acquisition of long-term monitoring images near the deep seafloor by Edokko Mark I.
367 (Available online at https://www.oceanbestpractices.net/handle/11329/359, accessed 30 June
368 2020)
369

370 Japan Meteorological Agency (2019a) A preliminary report on heavy rainfalls and strong winds
371 by Typhoon Hagibis (2019). (in japanese) (Available online at
372 https://www.data.jma.go.jp/obd/stats/data/bosai/report/2019/20191012/20191012.html, accessed
373 30 June 2020).

374

375 Japan Meteorological Agency (2019b) Data of Oceanographic and Marine Meteorological
376 Observation, (Available online at http://www.data.jma.go.jp/gmd/kaiyou/db/vessel_obs/data-
377 report/html/ship/ship_e.php, accessed 30 June 2020).

378

379 Kao S. J., Dai M., Selvaraj K., Zhai W., Cai P., Chen S. N., Yang J. Y. T., Liu J. T., Liu C. C.
380 and Syvitski J. P. M. (2010) Cyclone-driven deep-sea injection of freshwater and heat by
381 hyperpycnal flow in the subtropics. *Geophys. Res. Lett.* **37**, L21702.

382

383 Kasaya T., Mitsuzawa K., Goto T.-N., Iwase R., Sayanagi K., Araki E., Asakawa K., Mikada H.,
384 Watanabe T., Takahashi I. and Nagao T. (2009) Trial of Multidisciplinary Observation at an
385 Expandable Sub-Marine Cabled Station "Off-Hatsushima Island Observatory" in Sagami Bay,
386 Japan. *Sensors* **9**, 9241–9254.

387

388 Kawagucci S., Yoshida Y. T., Noguchi T., Honda M. C., Uchida H., Ishibashi H., Nakagawa F.,
389 Tsunogai U., Okamura K., Takaki Y., Nunoura T., Miyazaki J., Hirai M., Lin W., Kitazato H.
390 and Takai K. (2012) Disturbance of deep-sea environments induced by the M9.0 Tohoku
391 Earthquake. *Scientific Reports* **2**, 270.

392

393 Khripounoff A., Crassous P., Bue Lo N., Dennielou B. and Silva Jacinto R. (2012) Different
394 types of sediment gravity flows detected in the Var submarine canyon (northwestern
395 Mediterranean Sea). PROGRESS IN OCEANOGRAPHY 106, 138–153.

396

397 Lintern D. G., Hill P. R. and Stacey C. (2016) Powerful unconfined turbidity current captured by
398 cabled observatory on the Fraser River delta slope, British Columbia, Canada ed. P. Talling.
399 Sedimentology 63, 1041–1064.

400

401 Liu J. T., Wang Y.-H., Yang R. J., Hsu R. T., Kao S.-J., Lin H.-L. and Kuo F. H. (2012)
402 Cyclone-induced hyperpycnal turbidity currents in a submarine canyon. J. Geophys. Res. 117,
403 C04033, doi:10.1029/2011JC007630.

404

405 Meiburg E. and Kneller B. (2010) Turbidity Currents and Their Deposits. *Annu. Rev. Fluid*
406 *Mech.* **42**, 135–156.

407

408 Mikada H., Mitsuzawa K., Matsumoto H., Watanabe T., Morita S., Otsuka R., Sugioka H., Baba
409 T., Araki E. and Suyehiro K. (2006) New discoveries in dynamics of an M8 earthquake-
410 phenomena and their implications from the 2003 Tokachi-oki earthquake using a long term
411 monitoring cabled observatory. *Tectonophysics* **426**, 95–105.

412

413 Miwa, T., Y. Iino, T. Tsuchiya, M. Matsuura, H. Takahashi, M. Katsuragawa, T. Fukuba, Y.
414 Furushima, T. Fukuhara, T. Fukushima, and H. Yamamoto. 2016. Underwater Observatory
415 Lander for the Seafloor Ecosystem Monitoring using a Video System. Pages 333-336 *in* Techno-
416 Ocean. IEEE, Kobe.
417
418 Noguchi T., Tanikawa W., Hirose T., Lin W., Kawagucci S., Yoshida-Takashima Y., Honda M.
419 C., Takai K., Kitazato H. and Okamura K. (2012) Dynamic process of turbidity generation
420 triggered by the 2011 Tohoku-Oki earthquake. *Geochem. Geophys. Geosyst.* **13**, Q11003.
421
422 Normandeau A., Dietrich P., Hughes Clarke J., Van Wychen W., Lajeunesse P., Burgess D. and
423 Ghienne J. F. (2019) Retreat Pattern of Glaciers Controls the Occurrence of Turbidity Currents
424 on High-Latitude Fjord Deltas (Eastern Baffin Island). J. Geophys. Res. Earth Surf. 124, 1559–
425 1571.
426
427 Oguri K., Kawamura K., Sakaguchi A., Toyofuku T., Kasaya T., Murayama M., Fujikura K.,
428 Glud R. N. and Kitazato H. (2013) Hadal disturbance in the Japan Trench induced by the 2011
429 Tohoku–Oki Earthquake. *Scientific Reports* **3**, 1240–6.
430
431 Oka E., Ishii M., Nakano T., Suga T., Kouketsu S., Miyamoto M., Nakano H., Qiu B., Sugimoto
432 S. and Takatani Y. (2018) Fifty years of the 137°E repeat hydrographic section in the western
433 North Pacific Ocean. *Journal of Oceanography* **74**, 115–145.
434
435 Paull C. K., Talling P. J., Maier K. L., Parsons D., Xu J., Caress D. W., Gwiazda R., Lundsten E.
436 M., Anderson K., Barry J. P., Chaffey M., O'Reilly T., Rosenberger K. J., Gales J. A., Kieft B.,
437 McGann M., Simmons S. M., McCann M., Sumner E. J., Clare M. A. and Cartigny M. J. (2018)
438 Powerful turbidity currents driven by dense basal layers. Nature Communications, 1–9.
439
440 Piper D. J. W. and Normark W. R. (2009) Processes That Initiate Turbidity Currents and Their
441 Influence on Turbidites: A Marine Geology Perspective. *Journal of Sedimentary Research* **79**,
442 347–362.
443
444 Pohl F., Eggenhuisen J. T., Kane I. A. and Clare M. A. (2020) Transport and burial of
445 microplastics in deep-marine sediments by turbidity currents. *Environ. Sci. Technol.* **54**, 4180–
446 4189.
447
448 Pope E. L., Talling P. J., Carter L., Clare M. A. and Hunt J. E. (2017) Damaging sediment
449 density flows triggered by tropical cyclones. *Earth and Planetary Science Letters* **458**, 161–169.
450
451 Sassa K., He B., Miyagi T., Strasser M., Konagai K., Ostric M., Setiawan H., Takara K., Nagai
452 O., Yamashiki Y. and Tutumi S. (2012) A hypothesis of the Senoumi submarine megaslide in

453 Suruga Bay in Japan—based on the undrained dynamic-loading ring shear tests and computer
454 simulation. *Landslides* **9**, 439–455.
455
456 Sen, A., Dennielou, B., Tourolle, J., Arnaubec, A., Rabouille, C., & Olu, K. (2017). Fauna and
457 habitat types driven by turbidity currents in the lobe complex of the Congo deep-sea fan. Deep
458 Sea Research Part II: Topical Studies in Oceanography, 142, 167–179.
459
460 Sequeiros O. E., Pittaluga M. B., Frascati A., Pirmez C., Masson D. G., Weaver P., Crosby A.
461 R., Lazzaro G., Botter G. and Rimmer J. G. (2019) How typhoons trigger turbidity currents in
462 submarine canyons. Scientific Reports, 9, 9220, doi: 10.1038/s41598-019-45615-z.
463
464 Shizuoka Local Meteological Office, 2019: A preliminary climatological report on Typhoon #19,
465 Hagibis (2019). (in Japanese) (Available online at: https://www.jma-
466 net.go.jp/shizuoka/pdf/saigai/sokuhou20191017.pdf, accessed 18 June 2020).
467
468 Simmons S. M., Azpiroz Zabala M., Cartigny M. J. B., Clare M. A., Cooper C., Parsons D. R.,
469 Pope E. L., Sumner E. J. and Talling P. J. (2020) Novel Acoustic Method Provides First Detailed
470 Measurements of Sediment Concentration Structure Within Submarine Turbidity Currents. J.
471 Geophys. Res. Oceans 125, 1126–24.
472
473 Taira A. (2001) Tectonic evolution of the japanese island arc system. *Annu. Rev. Earth Planet.*
474 *Sci.* **29**, 109–134.
475
476 Takemi, T., and T. Unuma, 2020: Environmental factors for the development of heavy rainfall in
477 the eastern part of Japan during Typhoon Hagibis (2019). *SOLA*, **16**, 30−36, doi:
478 10.2151/sola.2020-006
479
480 Talling P. J., Paull C. K. and Piper D. J. W. (2013) How are subaqueous sediment density flows
481 triggered, what is their internal structure and how does it evolve? Direct observations from
482 monitoring of active flows. *Earth Science Reviews* **125**, 244–287.
483
484 Wang Z., Xu J., Talling P. J., Cartigny M. J. B., Simmons S. M., Gwiazda R., Paull C. K., Maier
485 K. L. and Parsons D. R. (2020) Direct evidence of a high-concentration basal layer in a
486 submarine turbidity current. Deep-Sea Research Part I 161, 103300.
487
488 Xu J.P. (2010) Normalized velocity profiles of field-measured turbidity currents, Geology, 38,
489 563–566, doi: 10.1130/G30582.1.
490
491 Zhang Y., Liu Z., Zhao Y., Colin C., Zhang X., Wang M., Zhao S. and Kneller B. (2018) Long-
492 term in situ observations on typhoon−triggered turbidity currents in the deep sea. *Geology* **46**,
493 675–678.

494

Supplementary File

496
497   Supplementary File 1: KawagucciSupplMovie.mp4
498   Supplementary File 2: data.xlsx

Figure 1

Topography around (A) Suruga Bay and (B) the Heda Canyon.

Red broken line shows a track of Typhoon Hagibis on 12 October 2019.
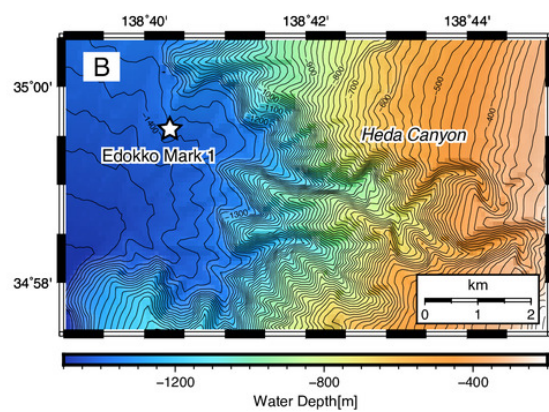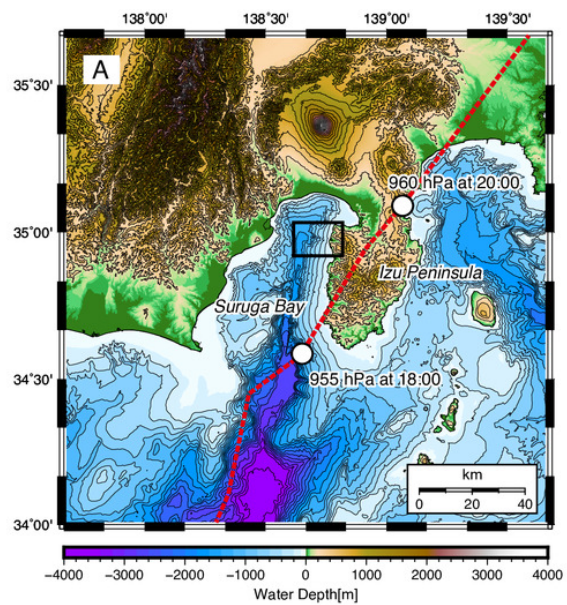
Figure 2

Edokko Mark 1.

(A) Composition and (B) Being deployed.
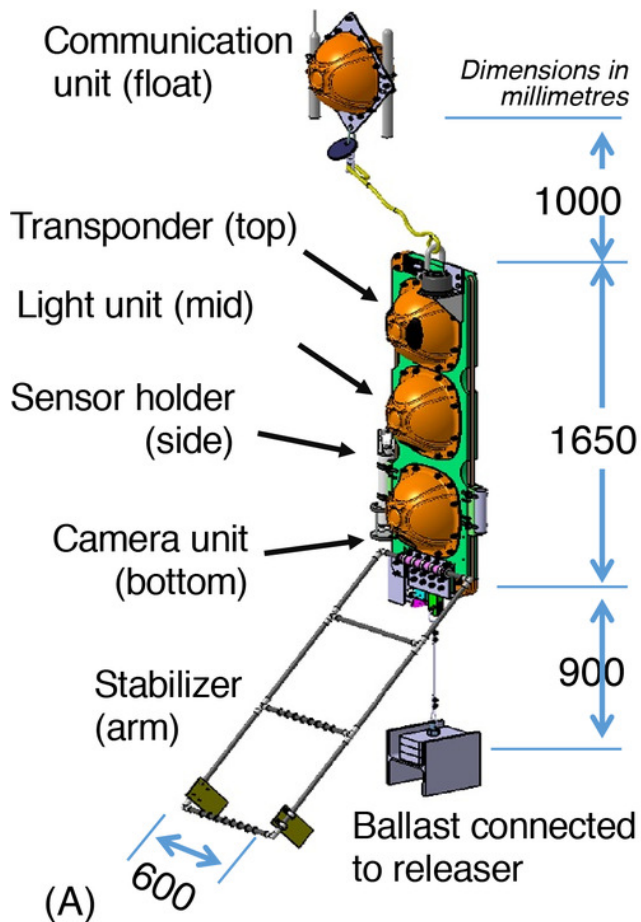
Figure 3

Temporal variation of parameters monitored by Edokko Mark 1.

(A) pressure with surface tide level, (B) turbidity, (C) RGB values of video images, (D) temperature, and (E) salinity.
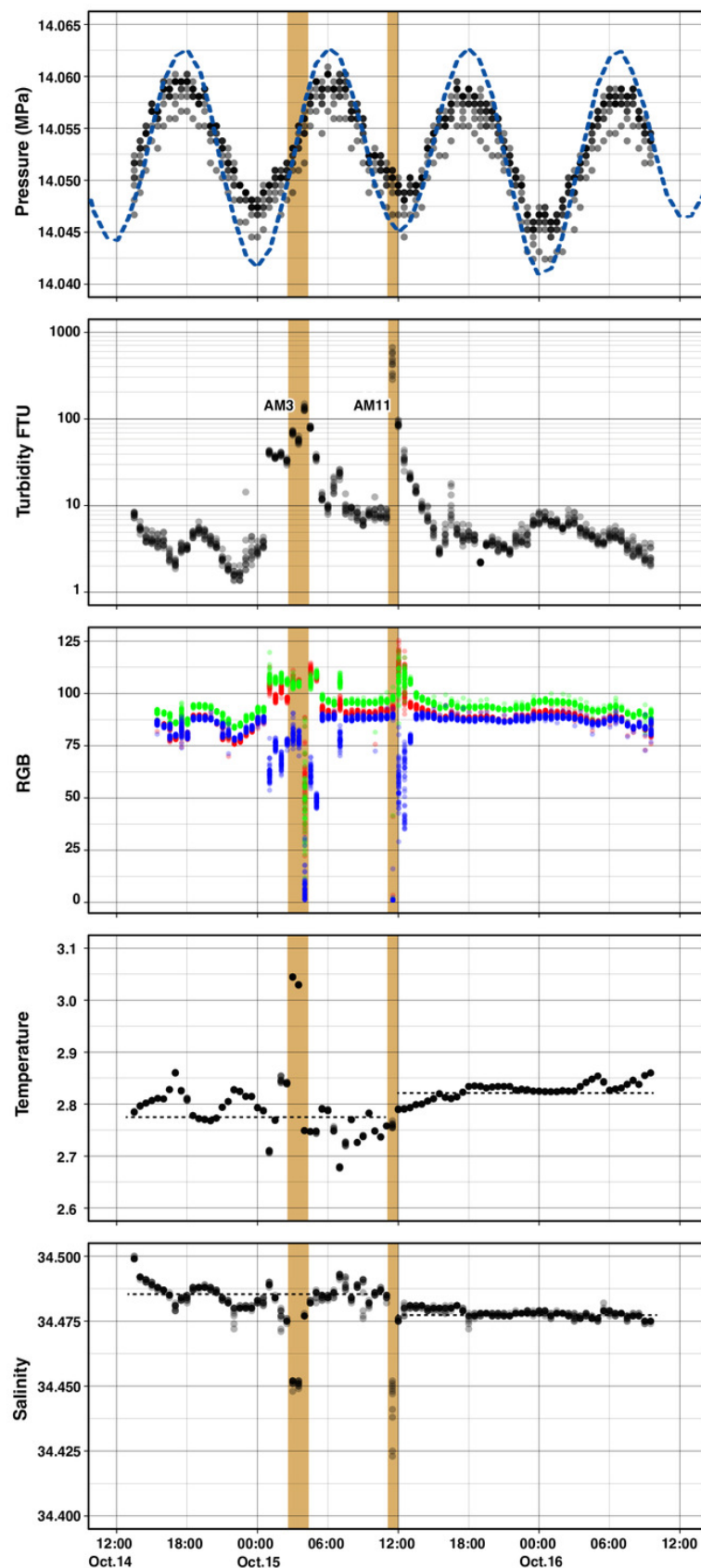
Figure 4

Representative images captured by the video camera on Edokko Mark 1.

Time of extracted images are shown on the frame grabs with panel name (A-J). A black horizontal bar was placed ~50 cm away from the video camera for distance indication.
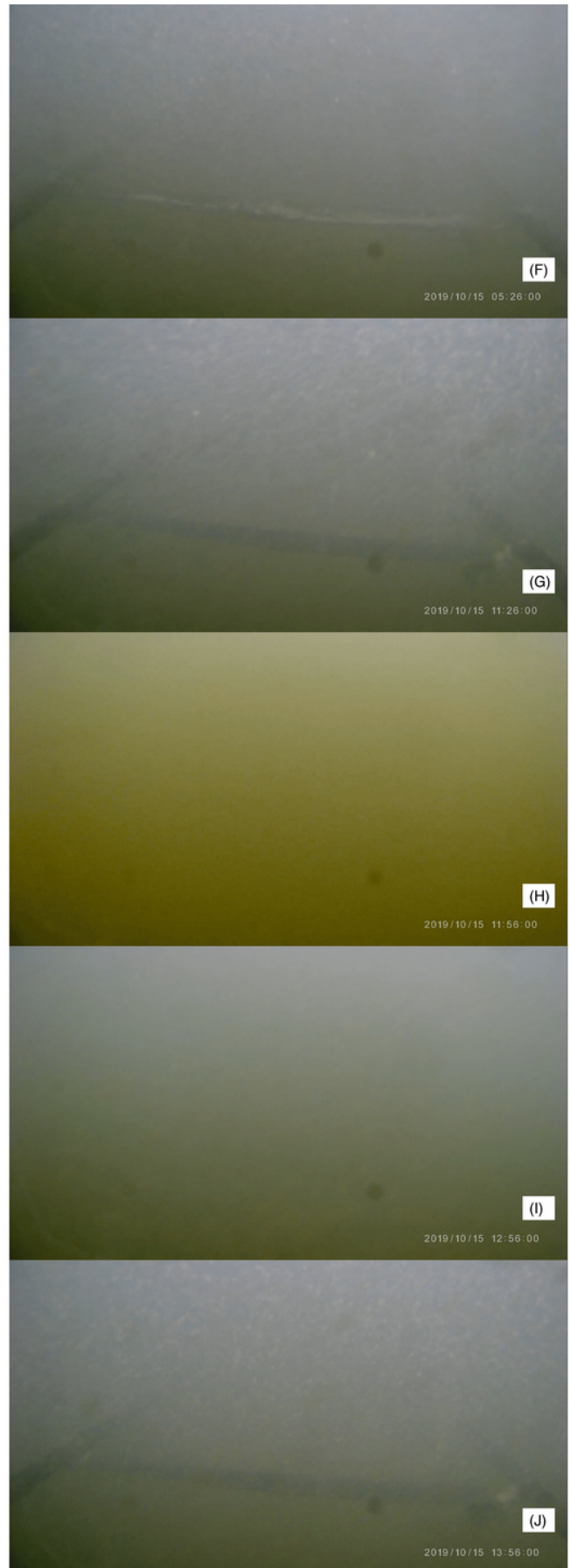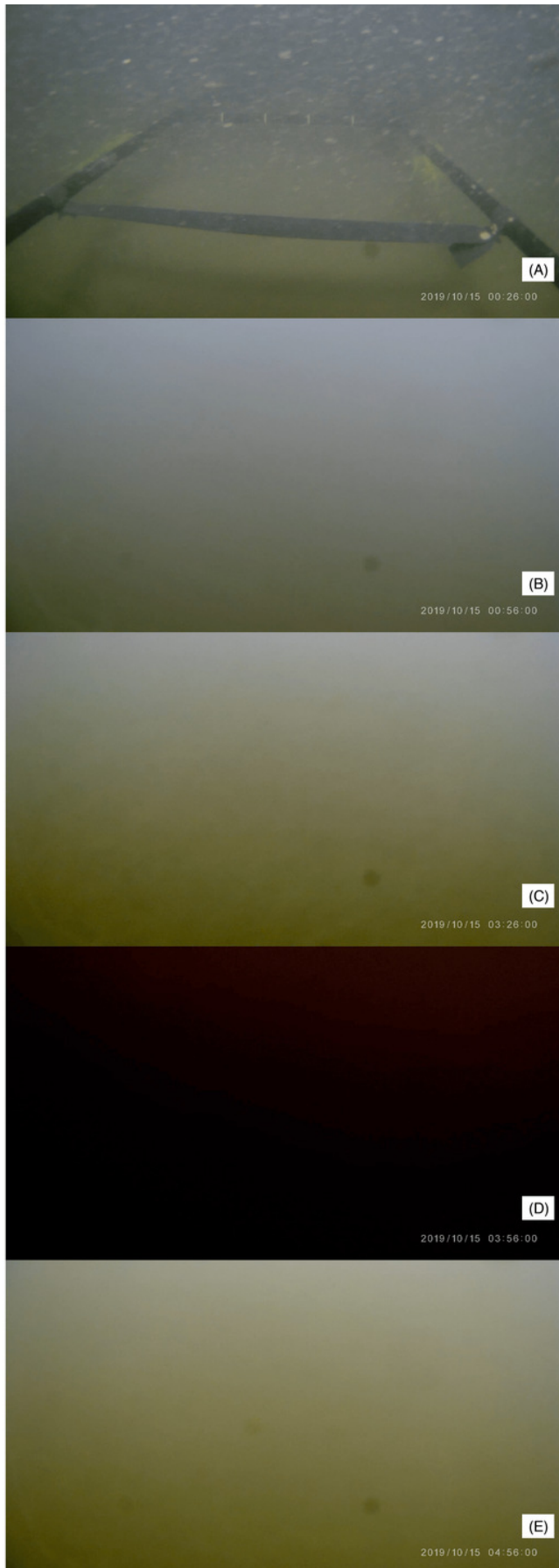
Figure 5

Figure 5: Sequential images during six seconds when a turbidity current struck Edokko Mark 1.
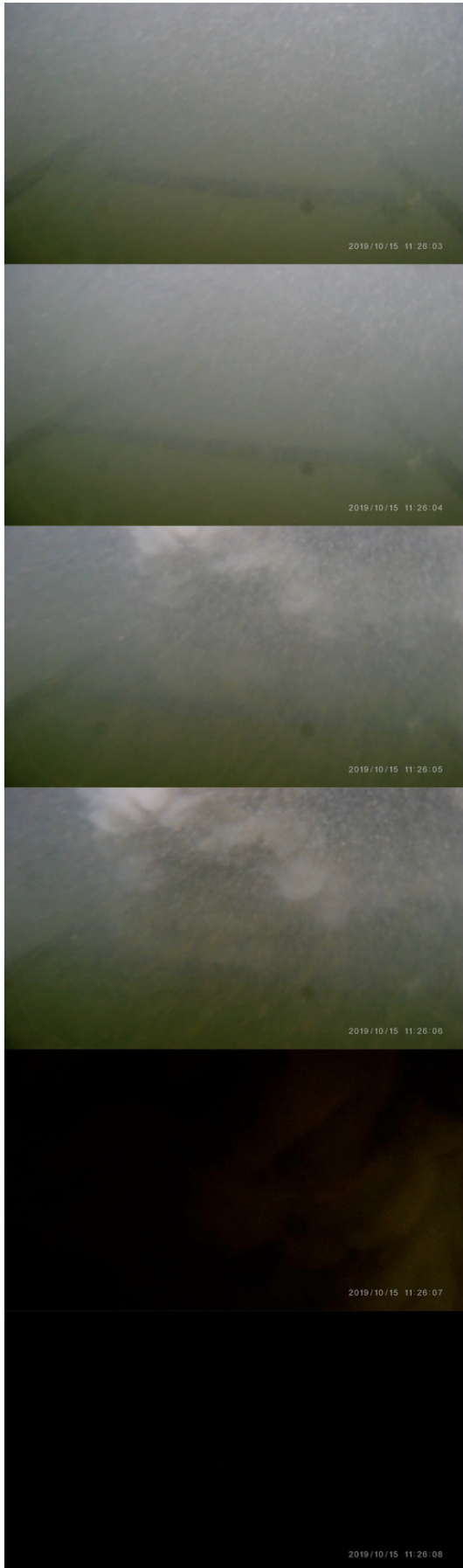
Figure 6

Seawater characteristics observed by XCTD (panels A-C), Edokko Mark 1, and the reference RF-6374 (panels D-E).